Experimental Demonstration of Plasma-Drag Acceleration of a Dust Cloud to Hypervelocities

C. M. Ticoş,[1] Zhehui Wang,[1] G. A. Wurden,[1] J. L. Kline,[1] D. S. Montgomery,[1] L. A. Dorf,[1] and P. K. Shukla[2]

[1]*Los Alamos National Laboratory, Plasma Physics Group P-24, Los Alamos, New Mexico 87545, USA*

[2]*Institut für Teoretische Physik IV, Fakültat für Physik und Astronomie, Ruhr-Universtät Bochum, D-44780 Bochum, Germany*

(Received 22 August 2007; published 17 April 2008)

Simultaneous acceleration of hundreds of dust particles to hypervelocities by collimated plasma flows ejected from a coaxial gun is demonstrated. Graphite and diamond grains with radii between 5 and 30 μm, and flying at speeds up to 3.7 km/s, have been recorded with a high-speed camera. The observations agree well with a model for plasma-drag acceleration of microparticles much larger than the plasma screening length.

DOI: 10.1103/PhysRevLett.100.155002 PACS numbers: 52.27.Lw, 52.30.−q, 52.70.Kz

Dust in plasmas has attracted a great deal of interest in the last two decades [1]. An important problem in dusty plasmas which has been a recent topic of intense research [2–8] is the plasma drag exerted on dust grains. The ion drag force exerted on dust grains smaller than the Debye length ($r_d \ll \lambda_D$) has been inferred from the deviation of free falling dust grains from their vertical trajectory as they passed through the bulk of a rf plasma [6], from the balance of forces acting on grains present in a dc discharge with drifting ions [7], or in microgravity conditions where a void is formed inside the dust cloud [8]. The results agreed well for ion trajectories given by the orbital-motion-limited (OML) theory [9]. However, for $r_d \gg \lambda_D$ experiments which focus on the plasma-drag force have been carried out only recently [10].

In typical laboratory dusty plasmas, the dust dynamics is dominated by electrostatic and gravity forces [11]. The plasma environment where plasma drag is dominant and dust acceleration is orders of magnitude higher than $g = 9.81\ \mathrm{m/s^2}$ requires charged particle densities of at least $10^{19}\ \mathrm{m^{-3}}$, and sufficient ion flow speeds [10,12]. Plasmas which meet these parameters are produced in coaxial guns [13] or near the wall of fusion reactors [14].

Highly accelerated microparticles can be used in micrometeorite impact studies [15], or as a diagnostic tool for mapping the magnetic field vectors in fusion reactors [16]. Hypervelocity dust has been detected by an electrostatic probe in the scrape-off-layer of tokamak plasma [17]. Laboratory produced dusty-plasma flows can be of relevance in astrophysics, by simulating the conditions of stellar jets' interactions with microparticle clouds [18]. The plasma-drag force is an essential aspect of plasma-dust interaction. For instance, the drag exerted by ion flow plays a key role in the formation of plasma crystals [19] or in the excitation of dust acoustic waves [1].

In this Letter we study experimentally plasma drag on microparticles in a new plasma regime, with ion temperatures of a few eV and 6 to 8 orders of magnitude higher density ($\sim 10^{22}\ \mathrm{m^{-3}}$) than in commonly produced dusty plasmas. Plasma drag is the dominant force acting on dust and is responsible for the simultaneous acceleration of hundreds of micron-size grains to speeds up to 3.7 km/s. The plasma flow is produced in a coaxial gun and expelled at ~25–60 km/s.

The plasmadynamic dust accelerator is presented in Fig. 1; more details about the experimental setup are given in Ref. [20]. Two types of dust powders manufactured by Alfa Aesar are used: diamond particles with radii $20 \leq r_d \leq 30\ \mu$m and density $\rho_d = 3.52\ \mathrm{g/cm^3}$ and graphite particles with $0.5 \leq r_d \leq 22\ \mu$m and $\rho_d = 2.25\ \mathrm{g/cm^3}$. The grains stored in a reservoir are released at the muzzle of the coaxial gun as a discharge is initiated. The coaxial gap is filled with deuterium from a plenum at 11.5 atm. The neutral gas then flows out of the gun at the sound speed into the acceleration channel (Fig. 1). After 1 ms the discharge is fired and the grains are highly accelerated by the plasma flow.

Breakdown of the gas occurs in $\approx 5\mu$s as an ignitron closes the circuit between the gun and a charged 1 mF capacitor bank. The discharge current reaches peak amplitudes in the range 100 to 250 kA, for electrode voltages between 5 and 10 kV. An image of the plasma flow captured by a high-speed video camera (DiCam Pro, The Cooke Corp.) for a 10 kV shot is presented in Fig. 2(a). The

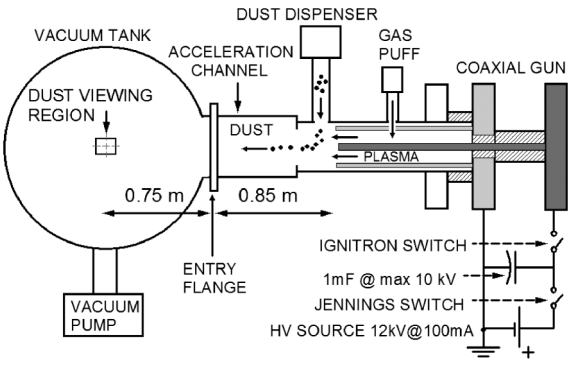

FIG. 1. Plasmadynamic dust accelerator: the gun and dust dispenser are not to scale relative to the tank; however, sizes are given for reference.

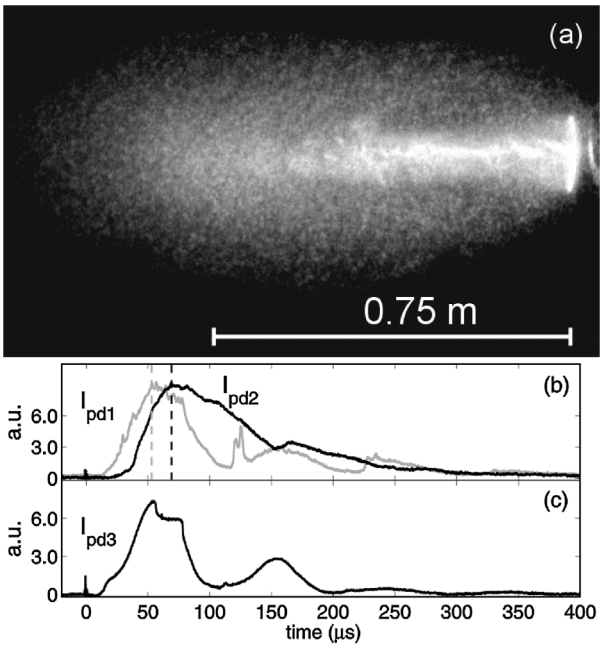

FIG. 2. A 10 kV shot: (a) image of plasma flow obtained using a fish-eye lens 16 mm $f/4$, for an exposure of 50 ns, (b) photodiode signals with perpendicular view on the flow, I_{pd1} and I_{pd2}, and (c) with end-on view inside the coaxial gap, I_{pd3}.

collimated plasma flow enters a vacuum tank with 1.5 m diameter, through a side port.

The plasma flow speed is deduced from optical measurements. A photodiode I_{pd1} with a side view records the white light emitted by the plasma at 0.25 m from the coaxial gun muzzle. A second photodiode I_{pd2} is placed 0.9 m downstream from the first one and also has a side view. From the time delay (16 ± 0.5 μs) between the peaks in their signals shown in Fig. 2(b), and their separating distance, a plasma flow speed $v_f = 56 \pm 2$ km/s is estimated. A third photodiode has an end-on view and looks into the coaxial gap of the plasma gun. Its signal I_{pd3} shown in Fig. 2(c) indicates a total shot duration of ≈ 400 μs. The plasma flow speed varies with the energy stored in the capacitor bank, as shown in Table I.

The line-integrated plasma density is determined from the Stark broadening of the D_α line at 0.25 m downstream from the gun muzzle, using streaked spectroscopy. The full width at half maximum is given by $\Delta\lambda_{1/2} = 0.54\alpha_{1/2}n_0^{2/3}$ (nm) [21], where $\alpha_{1/2} \approx 0.01$ and n_0 is the ion density in units of 10^{20} m^{-3}. The measured plasma density varies in time during a shot within the ranges given in Table I, which are determined by the discharge voltage. This method provides an average density over the whole cross section of the flow; the lower density layer at the flow edge may in fact reduce the width of the observed line. The bright filaments seen in Fig. 2(a) suggest there are regions in the flow where the density is higher, possibly due to the z-pinch effect which can constrict the flow. Thus the values presented in Table I are rather the lower limit of the actual plasma density.

TABLE I. Experimentally determined flow speed, plasma density, and ion temperature for different discharge voltages.

Voltage (kV)	v_f (km/s)	$n_i(\times 10^{22}$ m$^{-3})$	T_i (eV)
6	26 ± 0.5	$0.2–1.5 \pm 0.1$	1.3 ± 0.3
8	38 ± 1	$0.5–2.2 \pm 0.1$	1.7 ± 0.4
10	56 ± 2	$0.5–3.1 \pm 0.2$	2.8 ± 0.7

The ion temperature is inferred from observations of the expansion angle of the plasma flow in the vacuum tank. The thermal speed of the ions v_{th} is identified with the plasma expansion speed perpendicular to the flow speed v_f, and is deduced by measuring the angle between the two speed vectors: $v_{\text{th}} = v_f \tan(\alpha)$. Thus, for the 10 kV shot and the plasma flow of Fig. 2(a), $v_f = 56 \pm 2$ km/s, $\tan(\alpha) = 0.29 \pm 0.05$, and $v_{\text{th}} = 16 \pm 3$ km/s, resulting in $T_i = 2.8 \pm 0.7$ eV. For the 6 kV and 8 kV shots the values are given in Table I. The higher speed flow in the axial direction indicates a supersonic flow with Mach numbers from 3 to 4.

Dust acceleration to hypervelocities is demonstrated by in-flight observation of grains moving at a maximum speed of ≈ 3.7 km/s. The hypervelocity dust is self-illuminated due to the intense heating by plasma ion and electron fluxes. Dust imaging is thus possible by employing a telephoto lens with 500 mm $f/4$. However, the camera-telephoto lens system can only resolve grains with radii of at least 5 μm [10]. The rapidly moving grains appear in Fig. 3 as glowing tracers. Some that are at the edge of the depth of view, which is about 4 cm, show up as thick "bullets." The detection region is an 11×14 cm rectangle, situated downstream of the plasma flow at 1.6 m from the gun exit.

For dust detection the camera exposure time is set for 2 to 16 μs. The time-of-flight technique is used to infer the speed of each grain. For instance, the measured dust traces of the flying dust grains shown in Fig. 3 vary from 0.2 to 0.9 cm. The speed of a grain is calculated from the length of its trace divided by the exposure time of 4 μs: $v_d \approx 0.5$ to 2.3 km/s. A statistics of dust speeds for a total number of $\approx 1.94 \times 10^3$ detected grains is shown in Fig. 4. As expected, at higher flow speeds and densities, the bulk of grains in the distribution shifts towards larger flying speed.

Dust acceleration is achieved in two stages, corresponding to neutral gas drag followed by plasma drag. A numerical analysis based on the throughput of the valve orifice and exit diameter of the coaxial gun shows that the neutral pressure increases to ≈ 8 torr in 10^{-4} s within the interelectrode gap and to ≈ 0.2 torr in ≈ 1 ms within the acceleration channel. The drag force exerted by the neutral gas flowing with its thermal speed well before pressure equilibration in the system is given by

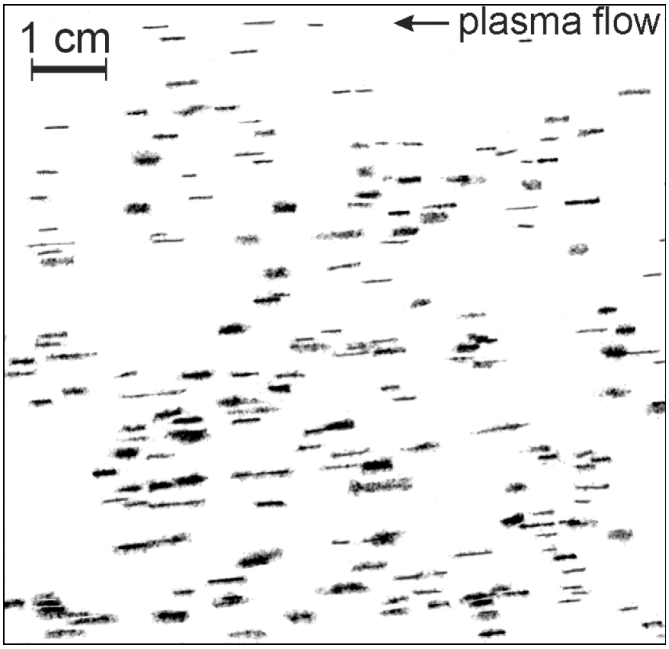

FIG. 3. Color-inverted image of self-glowing diamond grains flying along the direction of plasma flow.

$8/3\sqrt{2\pi}r_d^2 P_n \xi$, where P_n is the neutral gas pressure and $\xi(=1.5)$ is a factor which accounts for diffuse reflection of neutrals on the grain surface [1]. The pressure distribution in the acceleration channel is approximated during the 1 ms puff gas period with a function which decreases linearly with distance, from 8 torr at the gun muzzle to 0.2 torr at the end (0.85 m) of the acceleration channel.

In the second stage dust is accelerated by the plasma flow for a shot duration of 400 μs. A simulation of dust grain dynamics is performed using a plasma-drag model [12]. The electron and ion temperatures are assumed equal ($T_e = T_i$). The screening length given by the electron Debye length [3,4] is $\lambda_D \approx 10^{-7}$ m $\ll r_d$ and represents

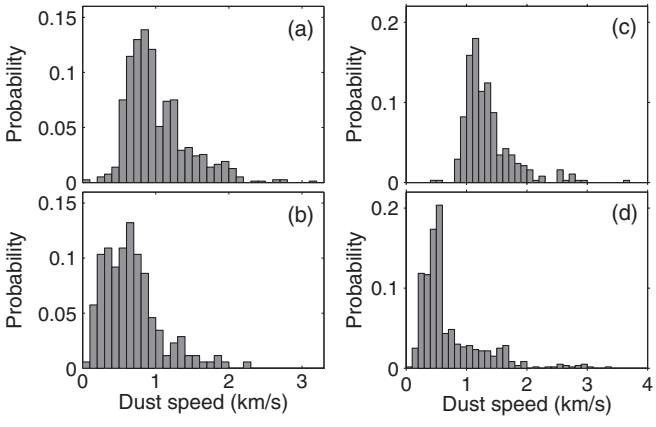

FIG. 4. Speed of diamond dust for (a) 10 kV shots and (b) 8 kV shots; speed of graphite dust for (c) 8 kV shots and (d) 6 kV shots.

one of the main features that distinguishes our dusty plasma from the strongly coupled regimes where $\lambda_D \gg r_d$. The grain potential consists of two regions: the thin sheath near the surface and a transition region—the presheath—which extends over a distance $\sim r_d$. The potential distribution in the presheath can be assumed spherical for a stationary plasma but it is expected to be anisotropic in supersonic plasma flow. Here we adopt the suggestion by Hutchinson [5] to estimate ion collection within the presheath in the stationary case, employing the OML theory [9]. A potential drop at the sheath-presheath edge $0.5k_B(T_i + T_e)$ is considered. In the force field of this potential, the angular momentum of ions is conserved. Ions with a critical angular momentum will graze the sheath edge instead of the grain surface. We suppose that all ions entering the sheath s_d, which has a width of a few λ_D, are absorbed on the grain surface. We discard here long-distance Coulomb interactions of ions with the grain. The ion collection radius is $b_c = (r_d + s_d)\sqrt{1+\chi}$, where $\chi = k_B(T_i + T_e)/m_i v_f^2$, and m_i is the ion mass. For our plasma parameters $\chi \leq 0.2$ and $b_c \cong r_d$ within 10%. The effect of the presheath attracting potential on ion collection is small and can be neglected. In the case of supersonic plasma flow which affects the symmetry of the potential [5,22], the angular momentum of ions is not conserved. It is expected that mostly ions with impact parameters $\lesssim r_d$ will be collected. Electron drag is neglected due to low electron mass. The ion and electron current densities at the sheath edge are $1/2en_i\sqrt{k_B(T_e+T_i)/m_i}$ and $1/2en_e(k_BT_e/2\pi m_e)^{-1/2}\exp(eV_d/k_BT_e)$, respectively, with the dust potential $V_d < 0$ and plasma density $n_e = n_i$. The equation of motion for a spherical grain dragged by the ion flow is

$$m_d \frac{dv_d}{dt} = 2\pi r_d^2 k_B T_i n_i G_0(s) \equiv F_c, \quad \text{with}$$

$$s = \sqrt{\frac{m_i(v_f - v_d)^2}{2k_BT_i}},$$

$$G_0(s) = \left(s^2 + 1 - \frac{1}{4s^2}\right)\mathrm{erf}(s) + \left(s + \frac{1}{2s}\right)\frac{\exp(-s^2)}{\sqrt{\pi}}.$$

Here m_d is the mass of a grain and v_d is the grain speed. We note that the ion drag force F_c, which is similar to that in the OML model of Ref. [5], represents the ion collection rate by the grain times the average ion momentum flux rate integrated over a shifted Maxwellian distribution function. The grain is heated by the electron and ion fluxes to its surface. The equations for temperature and charge variation in time are solved simultaneously with the equation of motion (see Ref. [12]) for the measured plasma flow speed and temperature. The ion density is taken constant and equal with the largest values shown in Table I. In the experiment no external magnetic fields are applied. The inductive electric fields estimated from the measured discharge currents are $\lesssim 10$ V/cm, while the electrostatic

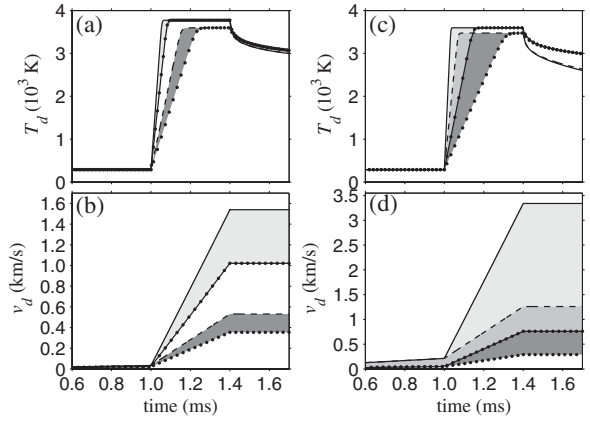

FIG. 5. Simulated dust temperature and speed: diamond in (a) and (b) and graphite in (c) and (d). The areas of (a) and (b) describe the behavior of grains with sizes from $r_d = 20$ μm (the upper bound) to $r_d = 30$ μm (the lower bound), while those of (c) and (d) are for grains with $r_d = 5$ μm to 22 μm. The light and dark gray areas in (a) and (b) correspond to 10 and 8 kV shots, while those in (c) and (d) are for 8 and 6 kV shots, respectively. The overlapping region is shown with medium dark gray.

electric field is perpendicular to the observed dust motion. The dust potential found numerically is $\sim -2.5kT_e$. In spite of intense thermionic emission, positive charging of grains was not directly verified in the present Letter. Dust acceleration in the flow direction by electric forces ($\lesssim 1$ m/s^2) is many orders of magnitude smaller than the acceleration due to the plasma-drag force ($2 \times 10^5 - 9 \times 10^6$ m/s^2).

The simulation starts with the period of gas puff, i.e., the interval [0 1] ms, during which dust is dragged by the neutral gas flow. The dust temperature remains constant, as shown in Figs. 5(a) and 5(c). The dust speed is presented in Figs. 5(b) and 5(d). Diamond dust [Fig. 5(b)] and large ($r_d = 22$ μm) graphite grains move with only 5–35 m/s due to their high mass, while the small graphite particles ($r_d = 5$ μm) reach ~210 m/s, as shown with the continuous and dashed lines in Fig. 5(d).

During the interaction with the plasma flow, i.e., the interval [1 1.4] ms, the grain temperature increases abruptly to 3550–3750 K for both types of dusts. For a 6 kV shot heating is slower for a large graphite grain with $r_d = 22$ μm, as demonstrated by the dotted line in Fig. 5(c). The speed of diamond dust ranges from 1.02 to 1.54 km/s for a 10 kV shot and from 0.35 to 0.53 km/s for an 8 kV shot. In the case of graphite dust the large distribution of sizes results in a wide range of speeds, from 0.75 to 3.35 km/s for an 8 kV shot and from 0.29 to 1.26 km/s for a 6 kV shot. After 1.4 ms, the dust speed achieved during plasma acceleration remains the same, and radiative cooling [$\propto r_d^2(T_d^4 - T_{\text{wall}}^4)$, $T_{\text{wall}} = 290$ K] leads to a slow decay of the dust temperature. The predicted values for dust speed are within the ranges of the measured ones, presented in Fig. 4. However, faster or slower moving dust grains can be observed in the experiment due to plasma density gradients that are present in the acceleration path [Fig. 2(a)].

In conclusion, it is demonstrated that the drag exerted by a collimated and dense plasma flow can accelerate a cloud of dust particles with a large size distribution to speeds up to several km/s.

This work was supported in part by the U.S. Department of Energy, under Contract No. DE-AC52-06NA25396, through the Office of Science.

[1] P. K. Shukla and A. A. Mamun, *Introduction to Dusty Plasma Physics* (Institute of Physics, Bristol, 2002); R. L. Merlino and J. A. Goree, Phys. Today **57**, No. 7, 32 (2004).
[2] M. S. Barnes *et al.*, Phys. Rev. Lett. **68**, 313 (1992).
[3] M. D. Kilgore *et al.*, J. Appl. Phys. **73**, 7195 (1993).
[4] S. A. Khrapak *et al.*, Phys. Rev. Lett. **90**, 225002 (2003); A. V. Ivlev *et al.*, Phys. Rev. Lett. **92**, 205007 (2004).
[5] I. H. Hutchinson, Plasma Phys. Controlled Fusion **47**, 71 (2005); *ibid.* **48**, 185 (2006).
[6] C. Zafiu *et al.*, Phys. Plasmas **10**, 1278 (2003).
[7] S. Ratynskaia *et al.*, Phys. Rev. Lett. **93**, 085001 (2004).
[8] M. Kretschmer *et al.*, Phys. Rev. E **71**, 056401 (2005).
[9] J. E. Allen, Phys. Scr. **45**, 497 (1992); M. Lampe, J. Plasma Phys. **65**, 171 (2001).
[10] Z. Wang, C. M. Ticos, and G. A. Wurden, Phys. Plasmas **14**, 103 701 (2007).
[11] D. A. Law *et al.*, Phys. Rev. Lett. **80**, 4189 (1998); E. Thomas, Jr. and J. Williams, *ibid.* **95**, 055001 (2005).
[12] C. M. Ticos *et al.*, Phys. Plasmas **13**, 103 501 (2006).
[13] U. Shumlak *et al.*, Phys. Rev. Lett. **87**, 205005 (2001); Z. Wang *et al.*, Rev. Sci. Instrum. **76**, 033501 (2005).
[14] A. L. Roquemore *et al.*, Rev. Sci. Instrum. **77**, 10E526 (2006); R. D. Smirnov *et al.*, Plasma Phys. Controlled Fusion **49**, 347 (2007); D. L. Rudakov *et al.*, J. Nucl. Mater. **363**, 227 (2007).
[15] E. B. Igenbergs and E. L. Shriver, J. Appl. Phys. **44**, 2177 (1973).
[16] Z. Wang *et al.*, IEEE Trans. Plasma Sci. **34**, 242 (2006).
[17] C. Castaldo *et al.*, Nucl. Fusion **47**, L5 (2007); S. Ratynskaia *et al.*, *ibid.* **48**, 015006 (2008).
[18] C. K. Goertz, Rev. Geophys. **27**, 271 (1989); A. L. Graps *et al.*, Nature (London) **405**, 48 (2000).
[19] H. M. Thomas and G. E. Morfill, Nature (London) **379**, 806 (1996).
[20] C. M. Ticos *et al.*, Rev. Sci. Instrum. **77**, 10E304 (2006).
[21] I. H. Hutchinson, *Principles of Plasma Diagnostics* (Cambridge University Press, Cambridge, England, 2002).
[22] P. C. Stangeby and J. E. Allen, J. Plasma Phys. **6**, 19 (1971).